



Short communication

Tropospheric SO₂ and NO₂ in 2012–2018: Contrasting views of two sensors (OMI and OMPS) from spaceYi Wang^{a, **}, Jun Wang^{a, b, *}^a Interdisciplinary Graduate Program in Informatics, The University of Iowa, Iowa City, IA, 52242, USA^b Department of Chemical and Biochemical Engineering, Center for Global & Regional Environmental Research, The University of Iowa, Iowa City, IA, 52242, USA

HIGHLIGHTS

- SO₂ and NO₂ trends and frequency distributions from OMPS and OMI are compared.
- Qualitatively consistent for upward trend in China and downward trend in India.
- Quantitative differences in trend and sign exist in developed countries.
- SO₂ and NO₂ signals for remote sensing are weakening in many parts of world.
- Reconciling OMI and OMPS product differences is emergently important.

ARTICLE INFO

Keywords:

SO₂
NO₂
OMPS
OMI
Inconsistent trends

ABSTRACT

The global long-term Climate Data Records (CDRs) of atmospheric SO₂ and NO₂ have been obtained from multiple satellite sensors since 1990s, and all these CDRs show consistently decreasing trends in developed countries and increasing trends in developing countries prior to 2010. However, much less clear is the quantitative differences among these CDRs and how such differences affect the inferences for atmospheric SO₂ and NO₂ climatology in terms of their annual means as well as their frequency distributions. Here, we compare and contrast the CDRs from the aged OMI sensor (the flagship for measuring NO₂ and SO₂ since 2005) and the young OMPS sensor series (that started measuring NO₂ and SO₂ in 2012 and will continue in next 2–3 decades). We show that after 2012, the difference of average SO₂ between OMPS and OMI is 0.12 DU and it only decreases to 0.04 DU after bias correction, despite their consistence in spatial pattern. NO₂ CDRs from OMPS and OMI overall exhibit general agreement in both magnitude and spatial pattern. Furthermore, the CDR differences can lead to the opposite trend signs in developed countries and the difficulty to reconcile trend magnitude in developing countries. Notable consistence in trend signs does exist, regardless of radiative cloud fraction, mainly showing decline of SO₂ and NO₂ in China and increasing in India; much inconsistency is, however, found in many parts of developed countries. No SO₂ trends and inconsistent NO₂ trends are found over Europe, and notable differences are found over U.S. where OMI SO₂ and NO₂'s declining trends are consistent with surface observations, but OMPS SO₂, albeit its better spatial agreement with surface data, shows increasing trend. This study calls the importance to assess CDRs from different satellite sensors with the account of frequency distributions for extreme events. This importance is emergent as the atmospheric SO₂ and NO₂ amounts are closer to the uncertainties of satellite-based retrievals in developed countries and are or will be declining in developing countries in the coming decades, all of which make the detection of signs, magnitudes, and spatiotemporal dichotomy a challenge from space.

1. Introduction

SO₂ and NO₂ are the largest contributors to anthropogenic aerosols

(Seinfeld and Pandis, 2016). Hence, a Climate Data Record (CDR) describing their spatial and temporal variations has been shown to be critical for investigating atmospheric composition and climate change

* Corresponding author. Interdisciplinary Graduate Program in Informatics, The University of Iowa, Iowa City, IA, 52242, USA.

** Corresponding author.

E-mail addresses: yi-wang-4@uiowa.edu (Y. Wang), jun-wang-1@uiowa.edu (J. Wang).

<https://doi.org/10.1016/j.atmosenv.2019.117214>

Received 23 July 2019; Received in revised form 11 November 2019; Accepted 6 December 2019

Available online 11 December 2019

1352-2310/© 2019 Elsevier Ltd. All rights reserved.

especially as a result of aerosol radiative forcing (Myhre et al., 2013). Furthermore, these CDRs have been used to study processes such as emissions (Qu et al., 2017; Streets et al., 2013; Wang et al., 2016; Wang et al., 2019a; Wang et al., 2019b), deposition (Liu et al., 2017), transport (Zhou et al., 2012), chemistry (Valin et al., 2013), evaluation (Xu et al., 2013), and trends of atmospheric SO₂ and NO₂ (Kharol et al., 2015, 2017; Krotkov et al., 2016; Lamsal et al., 2015; Richter et al., 2005; Zhou et al., 2012). Here, according to National Research Council (2014), CDR is defined as “a time series of measurements of sufficient length, consistency and continuity to determine climate variability and change”, and hence, anthropogenic climate change is an inherent part of the CDR.

Satellites have been providing observation-based global SO₂ and NO₂ CDRs for more than two decades, which contrasts with ground in situ observational sites that are sparse and unevenly distributed in space. The global tropospheric Vertical Column Density (VCD) distributions of SO₂ and NO₂ were first retrieved by Global Ozone Monitoring Experiment (GOME) during 1996–2004 (Burrows et al., 1999; Lee et al., 2009; Martin et al., 2002), and are subsequently continued by two GOME-2 sensors since 2006 and 2011, respectively (Munro et al., 2016; Nowlan et al., 2011; Richter et al., 2011), by SCanning Imaging Absorption SpectroMeter for Atmospheric CHartography (SCIAMACHY) during 2002–2012 (Bovensmann et al., 1999; Lee et al., 2009), by Ozone Monitoring Instrument (OMI) since 2004 (Krotkov et al., 2017; Li et al., 2013), by two Ozone Mapping and Profiler Suite (OMPS) sensors since 2011 and 2017, respectively (Yang et al., 2013, 2014), and by TROPOspheric Monitoring Instrument (TROPOMI) since 2017 (Veefkind et al., 2012). The third OMPS is scheduled to launch in 2022 and will extend the long-term CDRs of SO₂ and NO₂ for the next 2–3 decades.

Observations from GOME, GOME-2, SCIAMACHY, and OMI have been widely applied to estimate SO₂ and NO₂ trends. However, in most past studies, only CDRs from single sensor were used to study corresponding SO₂ and NO₂ trend during the sub-period (usually no more than 10 years) of the past two decades, and the results varied by region and time period (Kharol et al., 2015; Kharol et al., 2017; Krotkov et al., 2016; Lamsal et al., 2015; Schneider et al., 2015; Schneider and van der A, 2012; Zhou et al., 2012). For studies that used CDRs from two or more sensors, with or without adjusting bias among CRDs, little attention was paid to quantitatively compare difference of these CDRs for their overlapped time period (Georgoulias et al., 2019; Ghude et al., 2009; Hilboll et al., 2013; Lin et al., 2019; Richter et al., 2005; van der A et al., 2006), or the only focus of these studies is the polluted regions (Zhang et al., 2017).

Despite the progress in trend analysis of SO₂ and NO₂ from GOME, GOME-2, SCIAMACHY, and OMI CDRs, outstanding questions remain especially regarding the consistencies or differences of trend sign and magnitude detected by different sensors, the impacts of cloud on trend detection, and the change of both species in terms of their frequency distribution or probability density functions that provide yield statistics of not only mean but also median and extreme values. Addressing these issues is critical due to three factors. Firstly, emission decline at slower pace over developed countries (Jiang et al., 2018) is expected to make weak trend signals that may or may not be consistently described by different satellite CDRs, which has not been studied in literature. Secondly, SO₂ and NO₂ CDRs are usually retrieved under all-sky conditions while the impact of cloud cover selection on trend detection is still unclear. Thirdly, past researches focused on analyzing trends of monthly or yearly mean rather than evolution of frequency of extreme SO₂ and NO₂ event while the latter is more meaningful for air quality scientific community. These problems are compounded as trend analysis of NO₂ and SO₂ after 2010 may be subject to large uncertainties caused by row anomalies (Schenkeveld et al., 2017) in aged OMI as well as the large differences in overpassing times of GOME, SCIAMACHY and GOME-2 (all in the morning) against OMI (in the afternoon). Fortunately, OMPS started observations in 2012 with the overpassing time that is only 15 minutes ahead of OMI, and in this work, we make the first attempt to address these issues by using concurrent measurements of tropospheric

VCD of SO₂ and NO₂ from OMI and OMPS during April 2012–July 2018.

2. Data

OMI and OMPS VCD products for SO₂ and NO₂ from NASA are used in this study, and their detailed description is provided in S1 and S2. Briefly, OMI SO₂ data retrieved by means of principal component analysis have the precision of 0.5 DU (1 DU = 2.69×10^{16} molecules cm⁻²) (Li et al., 2013), which is a factor of 2.5 lower than that of OMPS SO₂ (0.2 DU) retrieved through Direct Vertical Column Fitting (DVCF) algorithm (Yang et al., 2013). The better precision of OMPS SO₂ is possibly caused by the fact that OMPS uses a single detector array to cover 310 nm where strong SO₂ absorption exists, while the band is not used in OMI SO₂ retrieval due to channel split near 310 nm for OMI (Yang et al., 2013). OMI and OMPS NO₂ are retrieved through variation of differential optical absorption spectroscopy algorithm (Krotkov et al., 2017) and DVCF (Yang et al., 2014), respectively. Although the precision of NO₂ total slant column density is about 0.033 DU for both OMPS and OMI, tropospheric VCD precision is 0.011 DU for OMPS, which is better than 0.017 DU for OMI (Krotkov et al., 2017; Yang et al., 2014). The precision difference between OMPS and OMI tropospheric NO₂ VCD is caused by different Stratosphere-Troposphere Separation (STS) approaches; OMI STS approach uses a small window to smooth stratospheric VCD, leaving some intrinsic measurement noise in the tropospheric VCD (Yang et al., 2014).

Ground-based daily SO₂ and NO₂ measurements are obtained from U.S. EPA's Air Quality System Data Mart (<https://www.epa.gov/airdata>). SO₂ is measured through coulometry or UV fluorescence methods, and NO₂ is observed by chemiluminescence approach (Demerjian, 2000). The NO₂ observational method actually measures NO by decomposing NO₂ to NO, which could systematically lead to positive bias, as NO_x (all compounds that are products of the atmospheric oxidation of NO_x) will be also reduced to NO (Lamsal et al., 2015). However, the systematic positive has very small impacts on relative trend values (Silvern et al., 2019), let alone the sign of trend.

3. Methods

The OMI Level-3 SO₂ and NO₂ products at $0.25^\circ \times 0.25^\circ$ grids are processed to construct monthly mean datasets at $1^\circ \times 1^\circ$ grids through “drop-in-the-box” gridding method (Sun et al., 2018). $1^\circ \times 1^\circ$ (instead of $0.25^\circ \times 0.25^\circ$) grids are used as OMPS pixel size (50 km \times 50 km at nadir) is much larger than $0.25^\circ \times 0.25^\circ$ grids. In the OMI Level-3 products, only the pixels that are not affected by row anomalies and have little cloud contamination, or Radiative Cloud Fraction (RCF) < 0.2 and 0.3 for SO₂ and NO₂, respectively, are retained. To remove the impacts of transient SO₂ cloud, only retrievals that are less than 15 DU are used, although passive volcanic degassing signals still exists. For this research, we mainly focus on China, India, the U.S., Europe, equatorial Pacific ocean (10°S – 10°N , 120°W – 150°W), the regions to which volcanic sources do not contribute SO₂ except southern Europe (SO₂ source distribution is available at <https://so2.gsfc.nasa.gov/>). The same gridding approach and fixed RCF thresholds are applied to OMPS SO₂ and NO₂ except in the investigation of how cloud affects trends, in which RCF thresholds vary.

Trend analysis approach introduced by Weatherhead et al., 1998 is applied to all CDRs as well as in situ observations. This method not only detects linear trend with consideration of seasonal variabilities and noise, but also conduct statistical significant test of it. The linear trend analysis model is shown as

$$Y_t = \mu + S_t + \omega X_t + N_t \quad t = 1, 2, \dots, T \quad (1)$$

where Y_t is monthly mean time series of observational variables (SO₂ or NO₂), μ is the offset at the start of time series, T is the total number of month, $X_t = t/12$ is number of years, ω is the magnitude of linear trend

per year, $S_t = \sum_{j=1}^4 [\beta_{1j} \sin(2\pi jt/12) + \beta_{2j} \cos(2\pi jt/12)]$ represents seasonal variations, and N_t is noise that cannot be represented by the model. N_t is assumed as red noise and represented as $N_t = \varphi N_{t-1} + \varepsilon_t$, where φ is the autocorrelation between N_t and N_{t-1} and ε_t is white noise. The standard deviation of the yearly linear trend is represented as

$$\sigma_\omega = \frac{\sigma_N}{n^{3/2}} \sqrt{\frac{1+\varphi}{1-\varphi}} \quad (2)$$

where σ_N is the standard deviation of N_t , and n equals $T/12$. If the absolute value of ω/σ_ω is larger than 2, it indicates that the linear trend is at 95% confidence level.

4. Results

Global distributions of SO_2 and NO_2 from OMI and OMPS during April 2012–July 2018 are shown in Fig. 1. OMI and OMPS observe similar patterns with the largest SO_2 level over China and India, followed by Europe and the U.S., and the largest NO_2 level over China, followed by Europe, the U.S., and India. OMPS SO_2 VCD in global average is 0.129 DU, which is much larger than 0.004 DU of OMI; the NO_2 difference is smaller between OMPS and OMI counterparts with values of 0.023 DU and 0.017 DU, respectively. Despite good agreement in qualitative description of spatial distribution for both SO_2 and NO_2 , OMI and OMPS CDRs have significant differences in the magnitudes (Fig. 1), trends (Fig. 2), and seasonal variations (Fig. 3) at regional scale during April 2012–July 2018.

4.1. China and India

Consistent are the locations of hot spots for SO_2 and NO_2 over China and India (Fig. 1a–d), the two largest anthropogenic SO_2 and NO_x emitters in Asia (Janssens-Maenhout et al., 2015). Both OMI and OMPS observe the largest SO_2 loadings over the North China Plain (NCP), Sichuan basin (30° N, 105° E), and Eastern India (EI) (Fig. 1a and c). As to NO_2 , hot spots are over NCP, the Yangtze River Delta (megacity clusters), Sichuan basin, the Pearl River Delta (megacity clusters), EI, and New Delhi, India's capital (Fig. 1b and d).

Though consistent qualitatively, tropospheric VCD of SO_2 and NO_2 from the two sensors over NCP and EI show systemic differences quantitatively. The averages of OMPS SO_2 are 0.46 DU and 0.30 DU over the NCP and EI, respectively, which contrast with lower values of 0.27 DU and 0.14 DU for OMI (Fig. 1e and f). The Pearson correlation coefficients (R) between OMI and OMPS monthly mean SO_2 at $1^\circ \times 1^\circ$ grid cell are 0.56 (Fig. 1e) and 0.46 (Fig. 1f) over NCP and EI, respectively. OMPS shows stronger SO_2 seasonal variability than OMI with coefficient of variation (standard deviation over average) of monthly mean 0.34 and 0.33 over NCP and EI, respectively, which are much larger than 0.16 and 0.25 for OMI (Fig. 3). Unlike large SO_2 difference between OMI and OMPS, averages of OMI NO_2 retrievals over the NCP and EI are 0.38 DU (Fig. 1g) and 0.09 DU (Fig. 1h), respectively, only slightly larger than OMI counterparts of 0.33 DU (Fig. 1g) and 0.08 DU (Fig. 1h). Moreover, R of monthly averaged NO_2 between OMI and OMPS are as large as 0.94 (Fig. 1g) and 0.84 (Fig. 1h) over the NCP and EI, respectively. Comparable seasonal variability of NO_2 is detected by the two sensors over NCP (coefficient of variation of 0.43 and 0.47 for OMI and OMPS,

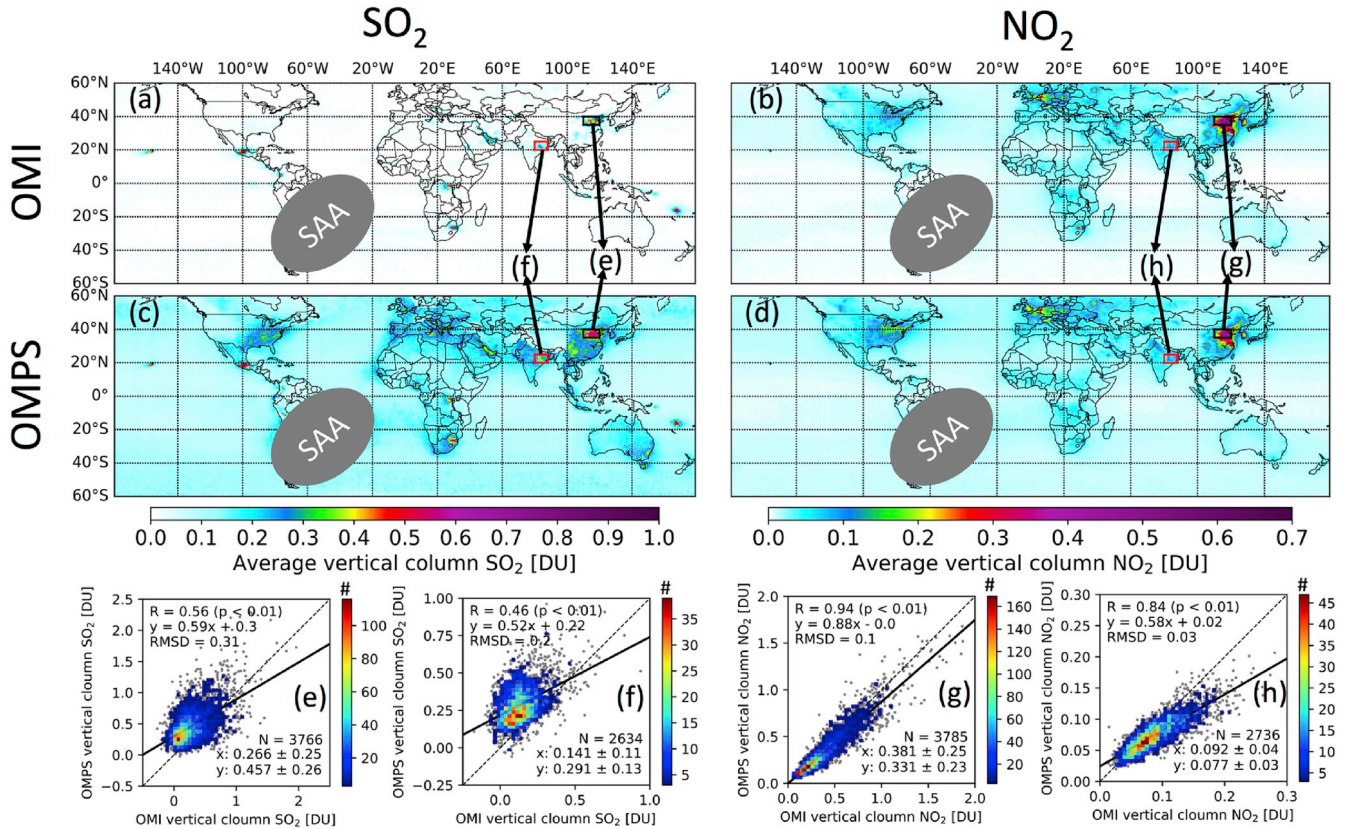


Fig. 1. Averages of VCD of OMI SO_2 (a) and NO_2 (b) and OMPS SO_2 (c) and NO_2 (d) during April 2012–July 2018. South Atlantic Anomaly (SAA) region is masked by grey ellipse. (e) and (f) are scatter plots of monthly average of OMPS SO_2 versus OMI SO_2 over North China plain (black box) and Eastern India (red box), respectively. (g) and (h) are similar to (e) and (f), respectively, but for NO_2 . Also shown on the scatter plots are 1:1 line (dash), linear regression line (solid), linear regression formula, Pearson correlation coefficient (R), p-value (p), root mean squared difference (RMSD), number of collocated pairs (N), OMI average and standard deviation (x), OMPS average and standard deviation (y), and density of collocated pairs (colorbar). (For interpretation of the references to color in this figure legend, the reader is referred to the Web version of this article.)

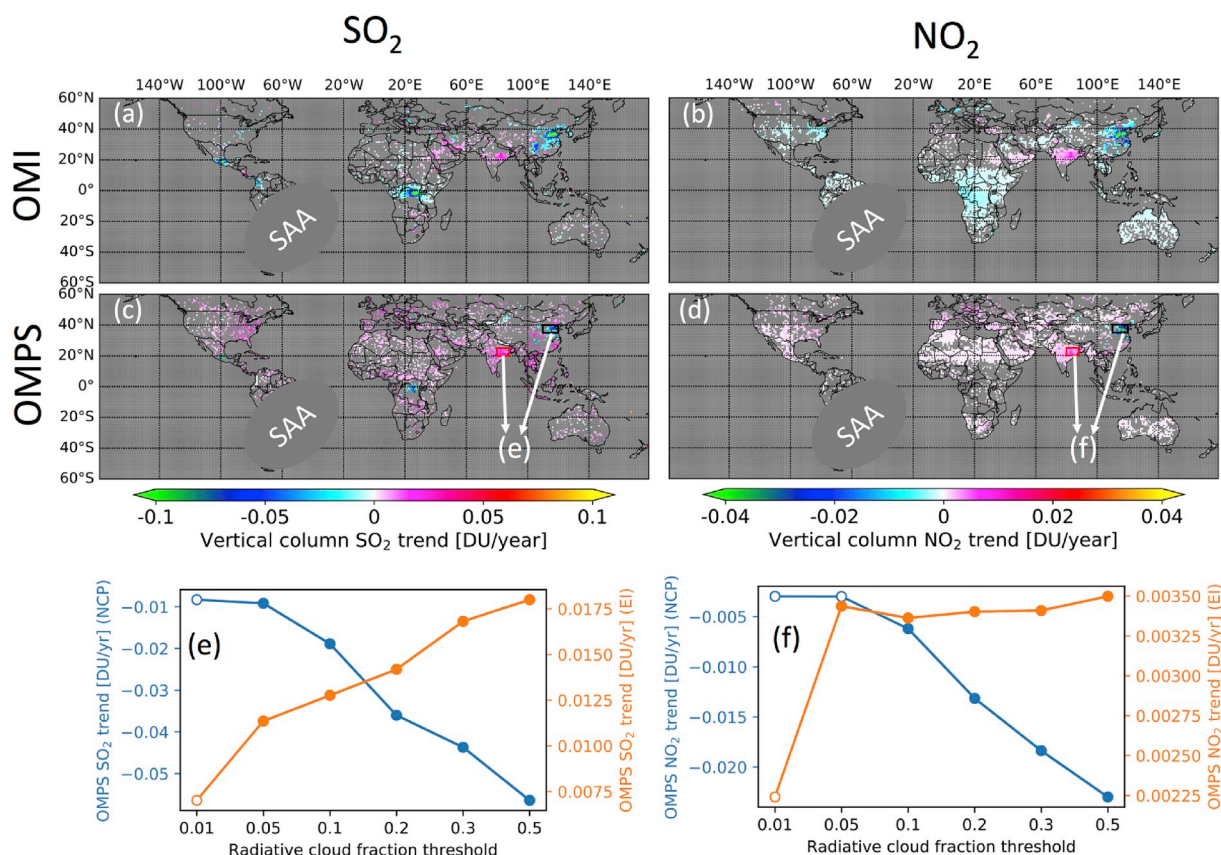


Fig. 2. Trends of VCD of OMI SO₂ (a) and NO₂ (b) and OMPS SO₂ (c) and NO₂ (d) during April 2012–July 2018. Only pixels that show trends at 95% confidence level and over land are shown. South Atlantic Anomaly (SAA) region is masked by grey ellipse. (e) and (f) are trends of OMPS SO₂ and NO₂, respectively, over North China Plain (NCP) and Eastern India (EI) at various radiative cloud fraction thresholds. Trends that are at 95% confidence level and not are shown by solid circles and open circles, respectively.

respectively) as well as EI (coefficient of variation of 0.22 and 0.21 for OMI and OMPS, respectively) (Fig. 3).

Despite systematic differences, OMI and OMPS SO₂ and NO₂ retrievals constantly show decreasing trends over China and increasing trends over India (Fig. 2a–d). Downward SO₂ trends are observed by both OMI and OMPS over the NCP (−0.069 DU/yr for OMI and −0.036 DU/yr for OMPS, shown in Fig. 4), the Sichuan basin (30° N, 105° E), and Xingjiang province (43° N, 85° E), although OMI detects more pixels with decreasing trends than OMPS (Fig. 2a and c). Over EI, both OMI and OMPS SO₂ retrievals observe upward trends (0.013 DU/yr for OMI and 0.014 DU/yr for OMPS, shown in Fig. 4), while OMPS detects more pixels with increasing trends than OMI (Fig. 2a and c). The contrasting SO₂ trends between NCP and EI could be a result of much higher rate of installation and operation of flue gas desulfurization over China than India (Krotkov et al., 2016; Wang et al., 2015). Moreover, India not only has overtaken U.S. as the world's second largest SO₂ emitting country in 2014 (Krotkov et al., 2016) but also is surpassing, if not already, China to be the world's largest SO₂ emitter in 2016 (Li et al., 2017), which is reflected by the downward trends over NCP and upward trends over EI that are detected by both OMI and OMPS. As for NO₂, both sensors observe strong decreasing trends over the NCP (−0.026 DU/yr for OMI and −0.018 DU/yr for OMPS, shown in Fig. 4), although OMI observes the weak downward trends that are not detected by OMPS over parts of Southern China (Fig. 2b and d). The penetration of denitration devices for coal-fired power plants and strict regulation for vehicle emissions should be primary reasons for these reductions (Liu et al., 2016). Conversely, stronger upward trends of NO₂ over EI (0.005 DU/yr for OMI and 0.003 DU/yr for OMPS, shown in Fig. 4) than Western India are detected by both OMI and OMPS (Fig. 2b and d), which should be mainly

ascribed to the increasing fuel consumption of coal-fired power plants without emission regulation in EI (Krotkov et al., 2016).

Trend signs detected by OMPS are independent of RCF, but trend magnitudes are positively correlated with RCF. OMPS SO₂ (NO₂) trends change from −0.008 DU/yr (−0.003 DU/yr) to −0.056 DU/yr (−0.023 DU/yr) over NCP and from 0.007 DU/yr (0.0022 DU/yr) to 0.018 DU/yr (0.0035 DU/yr) over EI as RCF threshold increases from 0.01 to 0.5. All these trends are at 95% confidence level when RCF threshold is no less than 0.1 (Fig. 2e–f).

To investigate the trends of extremely high monthly mean SO₂ and NO₂ loading, relative frequency distribution of the two trace gases over NCP and EI as a function of year are shown in Fig. 5. Over NCP, OMI and OMPS SO₂ maximums reduce from ~2.0 DU and ~2.6 DU in 2012 to ~0.6 DU and ~1.2 DU in 2017, respectively (Fig. 5a and b), in contrast to EI, where they increase from ~0.50 DU and ~0.55 DU to ~0.85 DU and ~0.95 DU, respectively (Fig. 5c and d). Not only OMI and OMPS SO₂ loading averages and medians show downward (upward) trends over NCP (EI), but also the relative frequencies of SO₂ larger than 0.5 DU decrease from 42.7% (47.1%) in 2012 to 0.2% (24.7%) in 2017 for OMI (OMPS) over NCP and increase from 0.0% (0.2%) to 2.9% (11.8%) over EI (Fig. 5a–d). As for NO₂, maximums of both OMI and OMPS are ~1.9 DU in 2012, reducing to ~1.2 DU and ~0.8 DU in 2017, respectively, over the NCP (Fig. 5e and f); conversely, they increase from ~0.17 DU and ~0.15 DU to ~0.27 DU and ~0.21 DU, respectively, over EI (Fig. 5g and h). Moreover, decreasing trends of NO₂ averages and medians over NCP and increasing trends over EI are also observed by the two sensors. Relative frequencies of NO₂ larger than 0.5 DU are 23.0% and 14.8% in 2017, down from 36.3% and 27.7% in 2012 for OMI and OMPS, respectively, over NCP, while NO₂ loadings over EI are persistently less

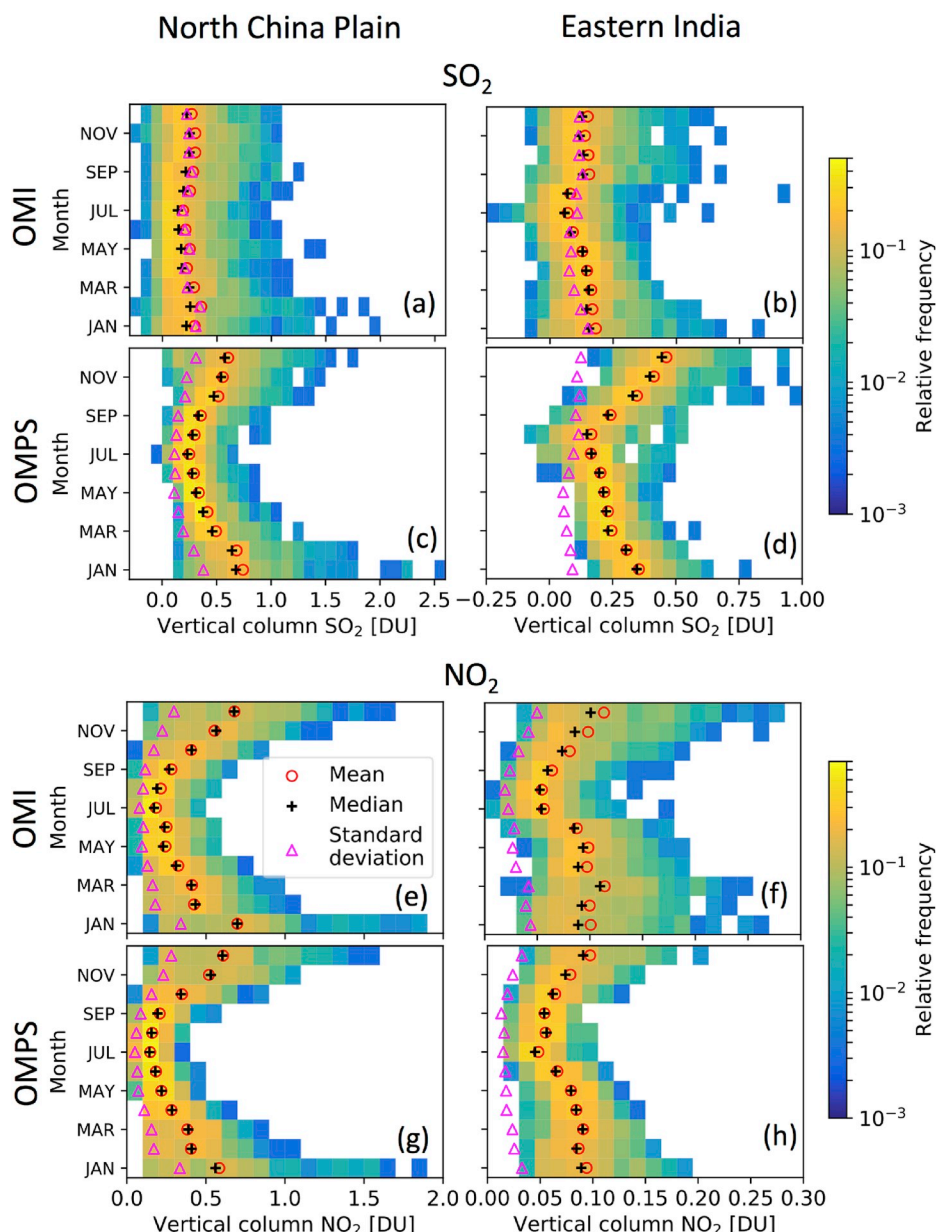


Fig. 3. (a) and (c) are relative frequency of OMI and OMPS SO₂ vertical column density (regridded in $1^\circ \times 1^\circ$ gridbox) as a function of month over Northern China Plain (black box in Fig. 1) during April 2012–March 2018, respectively. (b) and (d) are similar to (a) and (c), respectively, but for Eastern India (red box in Fig. 1). (e)–(h) are similar to (a)–(d), respectively, but for NO₂.

than 0.5 DU. If the threshold is 0.15 DU, relative frequencies over EI rise from 2.7% and 0.0% to 16.0% and 3.5% for OMI and OMPS, respectively.

4.2. U.S

In contrast to overall consistent finding over China and India, the averages of OMI and OMPS SO₂ retrievals sampled at EPA sites as well as their trends are quite different. EPA in situ SO₂ observations show hot spots over Illinois, Indiana, Ohio, and Pennsylvania states (Fig. 6a), where OMPS (Fig. 6b) also detects large SO₂, while OMI (Fig. 6c) does not. Moreover, the R between OMPS SO₂ retrievals and EPA in situ SO₂ observations is 0.27 ($p < 0.01$) while there is no correlation between OMI retrievals and EPA observations ($R = 0.08$, $p > 0.05$). OMPS SO₂ retrievals are in the range of 0.08–0.35 DU (Fig. 6c) which are much larger than OMI counterparts of being less than 0.07 DU. Although many EPA sites over eastern U.S. show decreasing trends of SO₂ (Fig. 6d), OMI

detects only downward trends at a small number of EPA sites over eastern U.S. and both upward and downward trends are detected by OMPS.

The typical SO₂ levels over the U.S. are quite low, and likely below the detection limit of OMI SO₂ retrieval algorithm, as illustrated by the lack of spatial correlation between OMI SO₂ and EPA in situ observations. While both OMI and OMPS have very stable performance over time with less than 0.5% degradation per year, long-term trends over regions with low SO₂ concentrations determined from OMI and OMPS retrievals may be impacted by small instrumental changes (Schenkeveld et al., 2017; Seftor et al., 2014), which have not yet been corrected in the OMI and OMPS products used in this investigation.

For NO₂, the averages of OMI and OMPS retrievals sampled at EPA sites are similar, while their trends are quite different. EPA observations, OMI retrievals, and OMPS retrievals all detect NO₂ hotspots around Los Angeles, Chicago and New York (Fig. 6g–i); the R values for EPA in situ observations with OMI and OMPS retrievals are 0.61 ($p < 0.01$) and 0.50

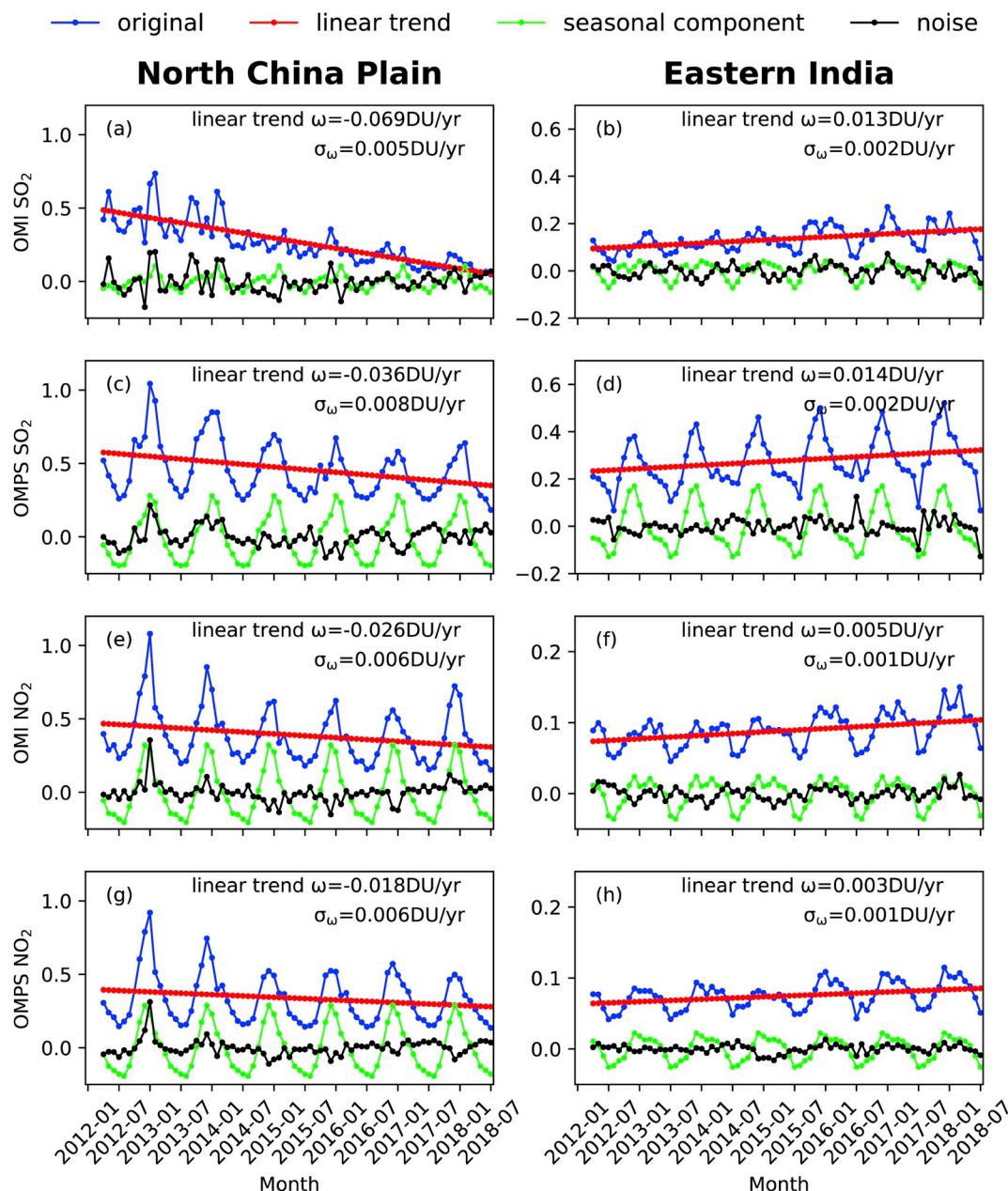


Fig. 4. Time series of monthly SO₂ and NO₂, and their decompositions over Northern China Plain (black box in Fig. 1) and Eastern India (red box in Fig. 1). (a) and (c) are SO₂ over Northern China Plain from OMI, OMPS, respectively. (e) and (g) are similar to (a) and (c) but for NO₂. (b), (d), (f), and (h) are similar to (a), (c), (e), and (g) but for Eastern India. Satellite vertical column density (blue line) is decomposed into linear trend (red line), seasonal component (green line), and noise (black line). Linear trend ω and its standard deviation σ_{ω} are shown. (For interpretation of the references to color in this figure legend, the reader is referred to the Web version of this article.)

($p < 0.01$), respectively. OMI and EPA consistently show decreasing trends; conversely, OMPS detects increasing trends.

4.3. Europe

OMPS SO₂ is larger than OMI over Europe, and neither of the two products shows significant trend. OMPS SO₂ is in the range of 0.15–0.25 DU (Fig. 1c) over almost all the Europe, which contrasts to the small values of less than 0.1 DU for OMI (Fig. 1a). OMPS observes large SO₂ levels over England, Bosnia and Herzegovina, Serbia, and Bulgaria, where large coal-fired power plants exist (Fioletov et al., 2016), and similarly, OMI also detects these hot spots except England. There are, however, no significant trend observed by either of the two products over these countries.

For NO₂, OMI and OMPS show a similar spatial pattern over Europe while trends are not always in accord. OMI and OMPS observe NO₂ hot spots around metropolises which include Manchester, Liverpool, and London in England, Amsterdam in Netherlands, Brussels in Belgium, Cologne, Frankfurt, and Berlin in Germany, Paris in France, and Moscow in Russia, and industrial areas around Milan in Italy and Katowice in Poland (Fig. 1b and d). Decreasing trends over areas around London in England, Amsterdam in Netherlands, Brussels in Belgium, Cologne and Frankfurt in Germany, Milan in Italy are detected by OMI while OMPS does not show trends in those regions (Fig. 2b and d). Both instruments, however, observe enhanced NO₂ levels over western Turkey (Fig. 2b and d).

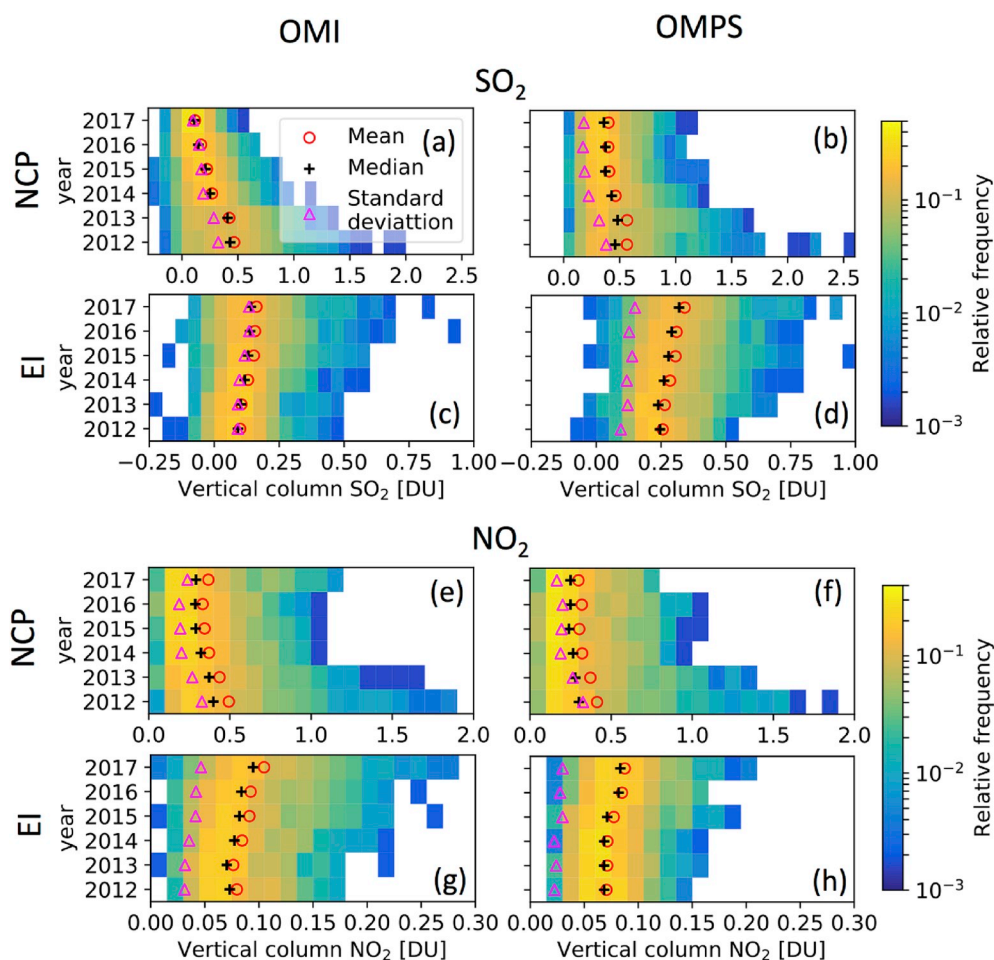


Fig. 5. (a) and (b) are relative frequency of OMI and OMPS SO_2 vertical column density (regrided in $1^\circ \times 1^\circ$ gridbox) as a function of year over Northern China Plain (NCP, black box in Fig. 1) during April 2012–March 2018, respectively. (c) and (d) are similar to (a) and (b), respectively, but for Eastern India (EI, red box in Fig. 1). (e)–(h) are similar to (a)–(d), respectively, but for NO_2 . (For interpretation of the references to color in this figure legend, the reader is referred to the Web version of this article.)

5. Discussion

SO_2 and NO_2 tropospheric VCD retrievals from OMI and OMPS are compared, which reveals their inconsistencies at different regions and seasons. Discussion of several factors that may or may not cause the differences of loadings and trend signs of SO_2 and NO_2 from both an algorithm and sensor characteristics point of view are provided below.

First, some differences can be explained by analyzing the bias and trends over the clean equatorial Pacific ocean (10°S – 10°N , 120°W – 150°W) where averages and trends of SO_2 and NO_2 are expected to be zero. Thus, the non-zero averages and trends are considered as systematic artifacts inherent in the algorithm. Positive OMPS SO_2 trends widely exist over remote clean ocean (Fig. S1c in the supporting information), and a positive trend of 8.9×10^{-4} DU/year (Fig. S2b) even exist over the clean equatorial Pacific ocean; in contrast, OMI observes both positive and negative SO_2 trends randomly exist over remote clean ocean (Fig. S1a), and the positive trend of 7.3×10^{-5} DU/year (Fig. S2a) over the clean equatorial Pacific ocean for OMI is much less than that derived from OMPS. For NO_2 over clean ocean, OMPS retrievals generally show positive trends (Fig. S1d), while OMI retrievals overall show negative trends (Fig. S1b); the NO_2 trends are 7.4×10^{-5} DU/year for OMPS (Fig. S2d) and -1.0×10^{-4} DU/year (Fig. S2c) for OMI. Thus, the positive SO_2 and NO_2 trends (artifacts) derived from OMPS may partly explain why (a) inconsistent NO_2 trends are found over Europe and (b) notable differences are found over U.S. where OMI SO_2 and NO_2 's declining trends are consistent with surface observations, but OMPS SO_2 , albeit its better spatial agreement with surface data, shows increasing trends.

Second, averages of SO_2 over the clean equatorial Pacific ocean

(10°S – 10°N , 120°W – 150°W) are 0.0035 DU for OMI and 0.0789 DU for OMPS (Fig. S2), and these values are considered as systematic bias. The differences of average SO_2 between OMPS and OMI are 0.12 DU globally and 0.2 DU over Eastern China; their counterparts, after bias correction, decrease to 0.04 DU and 0.12 DU respectively. Bias correction partly helps to reconcile the two products, but the large differences still exist.

Third, NO_2 fitting windows are 345–378 nm for OMPS and 402–465 nm for OMI, but such difference is not expected to lead to inconsistent NO_2 trends over the US and Europe between OMI and OMPS. NO_2 absorption cross sections have larger differential structures in the range of 402–465 nm than 345–378 nm, thus the fitting window of 402–465 nm is more suitable for retrieving NO_2 . In spite of this, Slant Column Density (SCD) precision is about 0.033 DU for both OMPS and OMI (Krotkov et al., 2017; Yang et al., 2014). OMI NO_2 SCD is retrieved by a DOAS approach and it is converted to VCD by a AMF. The OMI NO_2 AMF is assumed to be wavelength-independent. This assumption could lead to errors in the VCD, but we don't expect the error can change the sign of NO_2 trend. OMPS NO_2 is retrieved through Direct Vertical Column Fitting (DVCF) algorithm. In the DVCF approach, average AMF (or photon path lengths) for each wavelength, which is implicitly determined in the spectral fitting process is used. Thus, for OMPS NO_2 VCD, wavelength-dependent AMF is considered, and this is a key improvement of the DVCF approach over the DOAS method (Yang et al., 2014). However, DVCF method itself presumably won't lead to statistically significant trend in the retrieval products.

Fourth, aerosols are not considered in AMF calculation by the algorithms generating the data used in this study. This simplification may affect trend strength to some extent. McLinden et al. (2016) estimated that uncertainty of AMF due to aerosols is 10% by adjusting aerosol

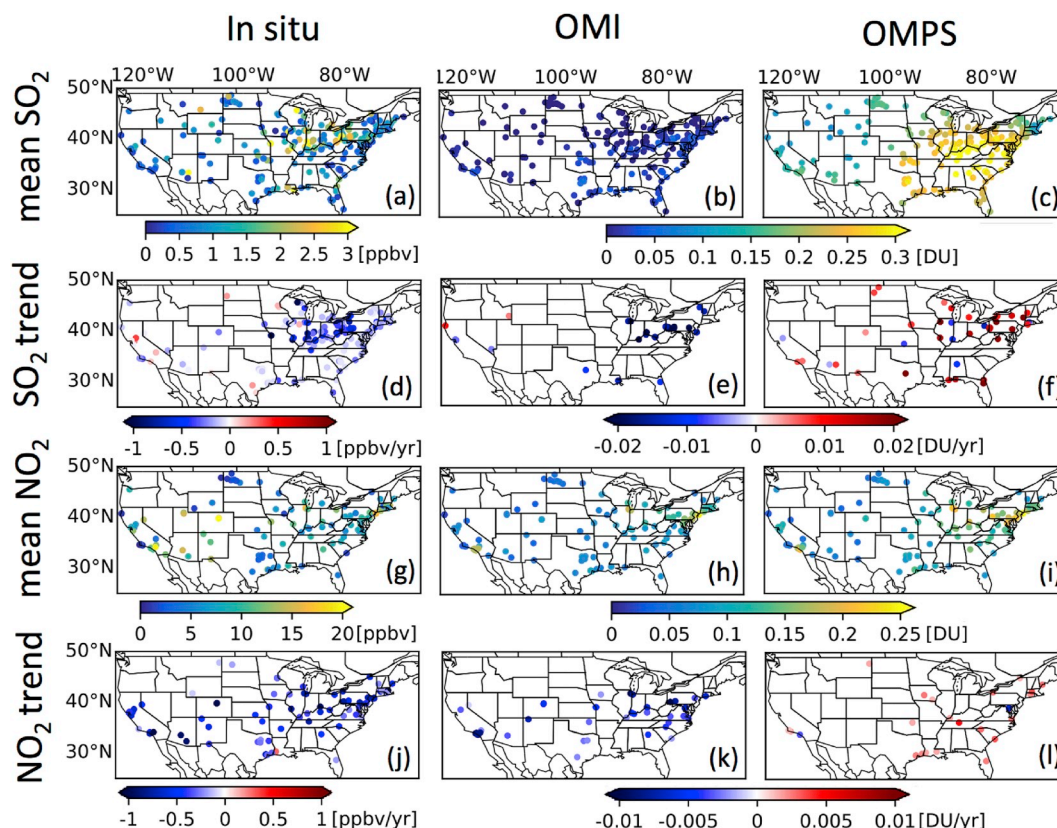


Fig. 6. (a) is averages of EPA in situ SO_2 during April 2012–December 2017. (b) and (c) are averages of OMI and OMPS SO_2 VCD sampled at EPA sites, respectively. (d), (e), and (f) are trends of EPA in situ SO_2 , OMI SO_2 VCD and OMPS SO_2 VCD, respectively. (g)–(l) are similar to (a)–(f), but for NO_2 . Only sites that show trends at 95% confidence level are plotted.

optical depth of ± 0.25 and recalculating AMFs. Considering AOD trends are less than 0.04 per year (or 0.25 during April 2012–July 2018) almost everywhere (except some regions over China and Western Asia) (Fig. S3), we can expect that the impact aerosol loading on SO_2 and NO_2 trends are less than 10% at most locations, which doesn't change the key results of our findings.

Finally, both systematic bias and random error can also be introduced in the SO_2 retrievals due to O_3 interference, which may affect trend analysis. Trends derived over the clean equatorial Pacific ocean (10°S – 10°N , 120°W – 150°W) (Fig. S2) can be considered as the lower limit of systematic bias over other regions. In the trend analysis, time series of original retrievals are decomposed into linear trend, seasonal component, and noise. The random error due to O_3 interference is expected in the noise part, thus they should not affect trend estimations, but affect standard deviations of trend.

In summary, the user guides for OMPS and OMI SO_2 and NO_2 data are followed in our analysis, and so a thorough analysis of the algorithm differences that contribute to the product difference is out the scope of this study that has a primary focus on the data analysis. For OMPS Level-2 product, we only use data labeled as good pixel. Data quality control has been applied to the generation of OMI Level-3 product from its Level-2 data, and consequently, all OMI Level-3 data are considered as good. Nevertheless, to reconcile the differences of SO_2 and NO_2 CDRs from different sensors and algorithms, algorithm inter-comparison studies supplemented with ground-based observations for validating the data products are needed.

6. Conclusions

Satellite-based CDRs for atmospheric SO_2 and NO_2 play an increasingly significant role in trend analysis. We compared CDRs of SO_2 and

NO_2 tropospheric VCD retrievals from OMI and OMPS during their overlapped period (2012–2018) and showed their consistencies and inconsistencies. The two sensors observe similar spatial distribution of SO_2 and NO_2 globally. OMPS SO_2 is much larger than OMI SO_2 in global average, while NO_2 difference is much smaller than SO_2 difference. The inconsistencies among CDRs can be caused by differences in sensors, calibration procedures, sampling processes, retrieval algorithms and spatial aggregation/averaging approaches (Levy et al., 2015), which should be addressed in future studies. The differences of magnitudes and trends observed by the two sensors vary by region.

Both OMI and OMPS observe large SO_2 and NO_2 levels over North China Plain as well as Eastern India, although OMI SO_2 is systemically lower than OMPS. Despite magnitude variation between OMI and OMPS, downward (upward) trends of mean, median, maximum, and the frequency of extreme event for SO_2 and NO_2 are detected by the two sensors over North China Plain (Eastern India). Radiative cloud fraction has no impact on trend signs, but is positively correlated with trend magnitudes.

OMI and OMPS NO_2 are spatial correlated with EPA in situ surface measurements over the U.S., but for SO_2 , only OMPS shows significant spatial correlation with EPA data. Downward trends of SO_2 and NO_2 are found by OMI, which are consistent with EPA surface observations, while OMPS mainly show upward trends for both SO_2 and NO_2 . Over Europe, SO_2 and NO_2 hot spots are observed by OMI and OMPS over metropolises and industrial areas. Although both show no SO_2 trends, OMI and OMPS NO_2 trends are not always in accord with each other.

Surface SO_2 and NO_2 levels have become low and stable in some regions of the U.S. and Europe. As a result, future research should focus on local areas around pollution sources, hence requiring data with higher spatial resolution. TROPOMI (Veefkind et al., 2012) was launched in 2017 and provides SO_2 and NO_2 retrievals with higher

spatial resolution (7 km \times 3.5 km) than both OMI (13 km \times 24 km) and OMPS (50 km \times 50 km). Considering the short lifetime of SO₂ and NO₂ in the troposphere, the importance of satellite observations will be enhanced by the launch of geostationary satellites which includes TEMPO (Zoogman et al., 2017) monitoring North America, Sentinel-4 (Ingmann et al., 2012) monitoring Europe, and GEMS (Kim, 2012) monitoring Eastern Asia in the near future. All these advancements will provide hourly SO₂ and NO₂ retrievals during daytime with high spatial resolution (2.1 km \times 4.4 km for TEMPO, 8.9 km \times 11.7 km for Sentinel-4, and 7 km \times 8 km for GEMS). These high-resolution data enable an unprecedented opportunity to investigate SO₂ and NO₂ variability in different spatiotemporal scale, thereby providing benchmarks to address OMPS-OMI trend differences revealed in this study, especially those over developed countries where pollutant levels are low and trend signals (if any) can be difficult to be sensed by the current generation of satellite sensors.

Author contribution

Jun Wang and Yi Wang: conceptualization, methodology, investigation, writing, reviewing, and editing. Yi Wang: data analysis, visualization, software. Jun Wang: supervision, resources, project administration, funding acquisition.

Declaration of competing interest

The authors declare that they have no known competing financial interests or personal relationships that could have appeared to influence the work reported in this paper.

Acknowledgements

This work was supported by NASA Aura Science Team and Atmospheric Modeling and Analysis program (grant #: NNX17AF63G managed by Dr. Kenneth Jucks and Dr. Richard Eckman) as well as TEMPO (Tropospheric Emissions: Monitoring of Pollution) satellite mission. Satellite data and in situ data shown in the paper can be obtained from NASA (<https://disc.gsfc.nasa.gov/>) and EPA (<https://www.epa.gov/outdoor-air-quality-data>), respectively. The results presented in this manuscript will be made available through Coalition on Publishing Data in the Earth and Space Sciences (<https://copdessdirectory.osf.io>) and please email J. Wang (jun-wang-1@uiowa.edu) for details.

Appendix A. Supplementary data

Supplementary data to this article can be found online at <https://doi.org/10.1016/j.atmosenv.2019.117214>.

References

- Bovensmann, H., Burrows, J.P., Buchwitz, M., Frerick, J., Noël, S., Rozanov, V.V., et al., 1999. SCIAMACHY: mission objectives and measurement modes. *J. Atmos. Sci.* 56 (2), 127–150.
- Burrows, J.P., Weber, M., Buchwitz, M., Rozanov, V., Ladstätter-Weissenmayer, A., Richter, A., et al., 1999. The global ozone monitoring experiment (GOME): mission concept and first scientific results. *J. Atmos. Sci.* 56 (2), 151–175.
- Demerjian, K.L., 2000. A review of national monitoring networks in North America. *Atmos. Environ.* 34 (12), 1861–1884.
- Fioletov, V.E., McLinden, C.A., Krotkov, N., Li, C., Joiner, J., Theys, N., et al., 2016. A global catalogue of large SO₂ sources and emissions derived from the Ozone Monitoring Instrument. *Atmos. Chem. Phys.* 16 (18), 11497–11519.
- Georgoulas, A.K., van der A, R.J., Stammes, P., Boersma, K.F., Eskes, H.J., 2019. Trends and trend reversal detection in 2 decades of tropospheric NO₂ satellite observations. *Atmos. Chem. Phys.* 6269–6294.
- Ghude, S.D., Van der A, R.J., Beig, G., Fadnavis, S., Polade, S.D., 2009. Satellite derived trends in NO₂ over the major global hotspot regions during the past decade and their inter-comparison. *Environ. Pollut.* 157 (6), 1873–1878.
- Hilboll, A., Richter, A., Burrows, J.P., 2013. Long-term changes of tropospheric NO₂ over megacities derived from multiple satellite instruments. *Atmos. Chem. Phys.* 13 (8), 4145–4169.
- Ingmann, P., Veihelmann, B., Langen, J., Lamarre, D., Stark, H., Courrèges-Lacoste, G.B., 2012. Requirements for the GMES atmosphere service and ESA's implementation concept: sentinels-4/-5 and -5p. *Remote Sens. Environ.* 120, 58–69.
- Janssens-Maenhout, G., Crippa, M., Guizzardi, D., Dentener, F., Muntean, M., Pouliot, G., et al., 2015. HTAP_v2.2: a mosaic of regional and global emission grid maps for 2008 and 2010 to study hemispheric transport of air pollution. *Atmos. Chem. Phys.* 15 (19), 11411–11432.
- Jiang, Z., McDonald, B.C., Worden, H., Worden, J.R., Miyazaki, K., Qu, Z., et al., 2018. Unexpected slowdown of US pollutant emission reduction in the past decade. *Proc. Natl. Acad. Sci.* 115 (20), 5099–5104.
- Kharol, S.K., Martin, R.V., Philip, S., Boys, B., Lamsal, L.N., Jerrett, M., et al., 2015. Assessment of the magnitude and recent trends in satellite-derived ground-level nitrogen dioxide over North America. *Atmos. Environ.* 118, 236–245.
- Kharol, S.K., McLinden, C.A., Sioris, C.E., Shephard, M.W., Fioletov, V., van Donkelaar, A., et al., 2017. OMI satellite observations of decadal changes in ground-level sulfur dioxide over North America. *Atmos. Chem. Phys.* 17 (9), 5921–5929.
- Kim, J., 2012. GEMS (Geostationary Environment Monitoring Spectrometer) onboard the GeoKOMPSAT to monitor air quality in high temporal and spatial resolution over Asia-Pacific Region. In: EGU General Assembly Conference Abstracts.
- Krotkov, N.A., Lamsal, L.N., Celarier, E.A., Swartz, W.H., Marchenko, S.V., Bucsela, E.J., et al., 2017. The version 3 OMI NO₂ standard product. *Atmos. Meas. Tech.* 10 (9), 3133–3149.
- Krotkov, N.A., McLinden, C.A., Li, C., Lamsal, L.N., Celarier, E.A., Marchenko, S.V., et al., 2016. Aura OMI observations of regional SO₂ and NO₂ pollution changes from 2005 to 2015. *Atmos. Chem. Phys.* 16 (7), 4605–4629.
- Lamsal, L.N., Duncan, B.N., Yoshida, Y., Krotkov, N.A., Pickering, K.E., Streets, D.G., Lu, Z., 2015. U.S. NO₂ trends (2005–2013): EPA air quality System (AQS) data versus improved observations from the ozone monitoring instrument (OMI). *Atmos. Environ.* 110 (Suppl. C), 130–143.
- Lee, C., Martin, R.V., van Donkelaar, A., O'Byrne, G., Krotkov, N., Richter, A., et al., 2009. Retrieval of vertical columns of sulfur dioxide from SCIAMACHY and OMI: air mass factor algorithm development, validation, and error analysis. *J. Geophys. Res.* 114 (D22), D22303.
- Levy, R.C., Munchak, L.A., Mattoo, S., Patadia, F., Remer, L.A., Holz, R.E., 2015. Towards a long-term global aerosol optical depth record: applying a consistent aerosol retrieval algorithm to MODIS and VIIRS-observed reflectance. *Atmos. Meas. Tech.* 8 (10), 4083–4110.
- Li, C., Joiner, J., Krotkov, N.A., Bhartia, P.K., 2013. A fast and sensitive new satellite SO₂ retrieval algorithm based on principal component analysis: application to the ozone monitoring instrument. *Geophys. Res. Lett.* 40 (23), 6314–6318.
- Li, C., McLinden, C., Fioletov, V., Krotkov, N., Carn, S., Joiner, J., et al., 2017. India is overtaking China as the world's largest emitter of anthropogenic sulfur dioxide. *Sci. Rep.* 7 (1), 14304.
- Lin, N., Wang, Y., Zhang, Y., Yang, K., 2019. A large decline of tropospheric NO₂ in China observed from space by SNPP OMPS. *Sci. Total Environ.* 675, 337–342.
- Yan, L., Liu, F., Zhang, Q., van der A, R.J., Zheng, B., Tong, D., et al., 2016. Recent reduction in NO_x emissions over China: synthesis of satellite observations and emission inventories. *Environ. Res. Lett.* 11 (11), 114002.
- Liu, L., Zhang, X., Xu, W., Liu, X., Lu, X., Chen, D., et al., 2017. Estimation of monthly bulk nitrate deposition in China based on satellite NO₂ measurement by the Ozone Monitoring Instrument. *Remote Sens. Environ.* 199, 93–106.
- Martin, R.V., Chance, K., Jacob, D.J., Kurosu, T.P., Spurr, R.J.D., Bucsela, E., et al., 2002. An improved retrieval of tropospheric nitrogen dioxide from GOME. *J. Geophys. Res.* 107 (D20), 4437.
- McLinden, C.A., Fioletov, V., Shephard, M.W., Krotkov, N., Li, C., Martin, R.V., et al., 2016. Space-based detection of missing sulfur dioxide sources of global air pollution. *Nat. Geosci.* 9 (7), 496–500.
- Munro, R., Lang, R., Klaes, D., Poli, G., Retscher, C., Lindström, R., et al., 2016. The GOME-2 instrument on the Metop series of satellites: instrument design, calibration, and level 1 data processing – an overview. *Atmos. Meas. Tech.* 9 (3), 1279–1301.
- Myhre, G., Shindell, D., Bréon, F.-M., Collins, W., Fuglestad, J., Huang, J., et al., 2013. Anthropogenic and natural radiative forcing. In: Stocker, T.F., Qin, D., Plattner, G.-K., Tignor, M., Allen, S.K., Boschung, J., Nauels, A., Xia, Y., Bex, V., Midgley, P.M. (Eds.), *Climate Change 2013: the Physical Science Basis. Contribution of Working Group I to the Fifth Assessment Report of the Intergovernmental Panel on Climate Change*. Cambridge University Press, Cambridge, United Kingdom and New York, NY, USA, pp. 659–740.
- National Research Council, 2004. *Climate Data Records from Environmental Satellites*. National Academies Press.
- Nowlan, C.R., Liu, X., Chance, K., Cai, Z., Kurosu, T.P., Lee, C., Martin, R.V., 2011. Retrievals of sulfur dioxide from the Global Ozone Monitoring Experiment 2 (GOME-2) using an optimal estimation approach: algorithm and initial validation. *J. Geophys. Res.* 116 (D18).
- Qu, Z., Henze, D.K., Capps, S.L., Wang, Y., Xu, X., Wang, J., Keller, M., 2017. Monthly top-down NO_x emissions for China (2005–2012): a hybrid inversion method and trend analysis. *J. Geophys. Res.* 122 (8), 4600–4625.
- Richter, A., Begoin, M., Hilboll, A., Burrows, J.P., 2011. An improved NO₂ retrieval for the GOME-2 satellite instrument. *Atmos. Meas. Tech.* 4 (6), 1147–1159.
- Richter, A., Burrows, J.P., Nüß, H., Granier, C., Niemeier, U., 2005. Increase in tropospheric nitrogen dioxide over China observed from space. *Nature* 437, 129.
- Schenkeveld, V.M.E., Jaross, G., Marchenko, S., Haffner, D., Kleipool, Q.L., Rozemeijer, N.C., et al., 2017. In-flight performance of the ozone monitoring instrument. *Atmos. Meas. Tech.* 10 (5), 1957–1986.
- Schneider, P., Lahoz, W.A., van der A, R., 2015. Recent satellite-based trends of tropospheric nitrogen dioxide over large urban agglomerations worldwide. *Atmos. Chem. Phys.* 15 (3), 1205–1220.

- Schneider, P., van der A, R.J., 2012. A global single-sensor analysis of 2002–2011 tropospheric nitrogen dioxide trends observed from space. *J. Geophys. Res.: Atmos.* 117 (D16).
- Seftor, C.J., Jaross, G., Kowitz, M., Haken, M., Li, J., Flynn, L.E., 2014. Postlaunch performance of the suomi national polar-orbiting partnership ozone mapping and profiler suite (OMPS) nadir sensors. *J. Geophys. Res.: Atmos.* 119 (7), 4413–4428.
- Seinfeld, J.H., Pandis, S.N., 2016. *Atmospheric Chemistry and Physics: from Air Pollution to Climate Change*, third ed. Wiley.
- Streets, D.G., Canty, T., Carmichael, G.R., de Foy, B., Dickerson, R.R., Duncan, B.N., et al., 2013. Emissions estimation from satellite retrievals: a review of current capability. *Atmos. Environ.* 77, 1011–1042.
- Silvern, R.F., Jacob, D.J., Mickley, L.J., Sulprizio, M.P., Travis, K.R., Marais, E.A., et al., 2019. Using satellite observations of tropospheric NO₂ columns to infer long-term trends in US NO_x emissions: the importance of accounting for the free tropospheric NO₂ background. *Atmos. Chem. Phys.* 19 (13), 8863–8878.
- Sun, K., Zhu, L., Cady-Pereira, K., Chan Miller, C., Chance, K., Clarisse, L., et al., 2018. A physics-based approach to oversample multi-satellite, multispecies observations to a common grid. *Atmos. Meas. Tech.* 11 (12), 6679–6701.
- Valin, L.C., Russell, A.R., Cohen, R.C., 2013. Variations of OH radical in an urban plume inferred from NO₂ column measurements. *Geophys. Res. Lett.* 40 (9), 1856–1860.
- van der A, R.J., Peters, D.H.M.U., Eskes, H., Boersma, K.F., Van Roozendaal, M., De Smedt, I., Kelder, H.M., 2006. Detection of the trend and seasonal variation in tropospheric NO₂ over China. *J. Geophys. Res.: Atmos.* 111 (D12).
- Veefkind, J.P., Aben, I., McMullan, K., Förster, H., de Vries, J., Otter, G., et al., 2012. TROPOMI on the ESA Sentinel-5 Precursor: a GMES mission for global observations of the atmospheric composition for climate, air quality and ozone layer applications. *Remote Sens. Environ.* 120, 70–83.
- Wang, S., Zhang, Q., Martin, R.V., Philip, S., Liu, F., Li, M., et al., 2015. Satellite measurements oversee China's sulfur dioxide emission reductions from coal-fired power plants. *Environ. Res. Lett.* 10 (11), 114015.
- Wang, Y., Wang, J., Henze, D.K., Zhou, M., Ge, C., Wang, W., 2019a. Inverse modeling of SO₂ and NO_x emissions over China from multi-sensor satellite data: 2. Downscaling for air quality forecasts. *Atmos. Chem. Phys. Discuss.* <https://doi.org/10.5194/acp-2019-880>.
- Wang, Y., Wang, J., Xu, X., Henze, D.K., Qu, Z., 2019b. Inverse modeling of SO₂ and NO_x emissions over China using multi-sensor satellite data: 1. formulation and sensitivity analysis. *Atmos. Chem. Phys. Discuss.* <https://doi.org/10.5194/acp-2019-879>.
- Wang, Y., Wang, J., Xu, X., Henze, D.K., Wang, Y., Qu, Z., 2016. A new approach for monthly updates of anthropogenic sulfur dioxide emissions from space: application to China and implications for air quality forecasts. *Geophys. Res. Lett.* 43 (18), 9931–9938.
- Weatherhead, E.C., Reinsel, G.C., Tiao, G.C., Meng, X.L., Choi, D., Cheang, W.K., et al., 1998. Factors affecting the detection of trends: statistical considerations and applications to environmental data. *J. Geophys. Res.: Atmos.* 103 (D14), 17149–17161.
- Xu, X., Wang, J., Henze, D.K., Qu, W., Kopacz, M., 2013. Constraints on aerosol sources using GEOS-Chem adjoint and MODIS radiances, and evaluation with multisensor (OMI, MISR) data. *J. Geophys. Res.: Atmos.* 118 (12), 6396–6413.
- Yang, K., Carn, S.A., Ge, C., Wang, J., Dickerson, R.R., 2014. Advancing measurements of tropospheric NO₂ from space: new algorithm and first global results from OMPS. *Geophys. Res. Lett.* 41 (13), 4777–4786.
- Yang, K., Dickerson, R.R., Carn, S.A., Ge, C., Wang, J., 2013. First observations of SO₂ from the satellite Suomi NPP OMPS: widespread air pollution events over China. *Geophys. Res. Lett.* 40 (18), 4957–4962.
- Zhang, Y., Li, C., Krotkov, N.A., Joiner, J., Fioletov, V., McLinden, C., 2017. Continuation of long-term global SO₂ pollution monitoring from OMI to OMPS. *Atmos. Meas. Tech.* 10 (4), 1495–1509.
- Zhou, Y., Brunner, D., Hueglin, C., Henne, S., Staehelin, J., 2012. Changes in OMI tropospheric NO₂ columns over Europe from 2004 to 2009 and the influence of meteorological variability. *Atmos. Environ.* 46, 482–495.
- Zoogman, P., Liu, X., Suleiman, R.M., Pennington, W.F., Flittner, D.E., Al-Saadi, J.A., et al., 2017. Tropospheric emissions: monitoring of pollution (TEMPO). *J. Quant. Spectrosc. Radiat. Transf.* 186, 17–39.